EglN3 hydroxylase stabilizes BIM-EL linking VHL type 2C mutations to pheochromocytoma pathogenesis and chemotherapy resistance

EglN3 hydroxylase stabilizes BIM-EL linking VHL type 2C mutations to pheochromocytoma pathogenesis and chemotherapy resistance

Shuijie Li[1], Javier Rodriguez[2], Wenyu Li[1], Petra Bullova[1], Stuart M. Fell[1], Olga Surova[1], Isabelle Westerlund[3], Danijal Topcic[3], Maria Bergsland[3], Adam Stenman[4], Jonas Muhr[3], Monica Nister[4], Johan Holmberg[3], C. Christofer Juhlin[4], Catharina Larsson[4], Alex von Kriegsheim[2], William G. Kaelin Jr[5] and Susanne Schlisio[1]

[1]Department of Microbiology, Tumor and Cell Biology, Karolinska Institutet, SE-17177, Stockholm, Sweden;

[2]Edinburgh Cancer Research Centre, IGMM, University of Edinburgh, Edinburgh EH4 2XR, UK

[3]Department of Cell and Molecular Biology, Karolinska Institutet, SE-17177, Stockholm, Sweden;

[4]Department of Oncology-Pathology, Cancer Center Karolinska, Karolinska Institutet, SE-17176 Stockholm, Sweden

[5]Department of Medical Oncology, Dana-Farber Cancer Institute and Brigham and Women's Hospital, Harvard Medical School, Boston, MA 02215, USA

Corresponding Author:

Susanne Schlisio, Ph.D.

Department of Microbiology and Tumor and Cell Biology, Karolinska Institutet, SE-17177, Stockholm, Sweden.

ABSTRACT

Despite the discovery of the oxygen-sensitive regulation of HIFα by the von Hippel-Lindau protein (VHL), the mechanisms underlying the complex genotype–phenotype correlations in VHL disease remain unknown. Some germline *VHL* mutations cause familial pheochromocytoma and encode proteins that preserve their ability to downregulate HIFα. While type 1, 2A and 2B *VHL* mutants are defective in regulating HIFα, type 2C mutants encode proteins that preserve their ability to downregulate HIFα. Here we identified a novel oxygen-sensitive function of VHL that is abolished by *VHL* type 2C mutations. We found that BIM-EL, a pro-apoptotic BH3-only protein, is hydroxylated by EglN3 and subsequently bound by VHL. VHL mutants fail to bind hydroxylated BIM-EL, regardless of whether they have the ability to bind hydroxylated HIFα or not. VHL binding inhibits BIM-EL phosphorylation by ERK kinase on serine 69. This causes BIM-EL to escape from proteasomal degradation, allowing it to enhance EglN3-induced apoptosis. BIM-EL was rapidly degraded in cells lacking wild-type VHL or in which EglN3 was inactivated genetically or by lack of oxygen, leading to enhanced cell survival and chemotherapy-resistance. Combination therapy using ERK inhibitors, however, resensitizes VHL- and EglN3-deficient cells that are otherwise cisplatin resistant.

KEYWORDS:
pheochromocytoma, paraganglioma, VHL-type-2C, O2-sensing, prolyl hydroxylation, EGLN3, apoptosis.

SIGNIFICANCE

Different mutations of the *VHL* tumor suppressor gene cause different subtypes of the von Hippel–Lindau hereditary cancer syndrome. Dysregulation of VHL's canonical substrate, HIFα, cannot fully explain the complex genotype-phenotype manifestation within the VHL disease. Here we describe a new oxygen-sensitive function of VHL that regulates hydroxylated BIM-EL protein stability during developmental apoptosis. We show type 2C VHL mutants, which cause pheochromocytoma and paraganglioma despite repressing HIFα, destabilize Bim-EL . Other genetic mutations linked to paraganglioma, similar to loss of Bim-EL, protect from apoptosis upon NGF withdrawal. It is therefore likely that dysregulation of BIM-EL contributes to the pathogenesis of VHL-related pheochromocytoma. Furthermore, loss of BIM-EL expression can lead to chemotherapy-resistance in other VHL related neoplasms and renders ccRCC cells insensitive to cisplatinum.

\body

INTRODUCTION

Von Hippel-Lindau Disease (VHL) is caused by germline mutations of the *VHL* gene and predisposes to a variety of tumors including haemangioblastoma (HB) of the retina and nervous system, clear renal cell carcinoma (ccRCC; the most common form of kidney cancer) and tumors of sympathoadrenal origin, such as pheochromocytoma/paraganglioma (PCC/PGL) (1). HIFα activation is necessary and sufficient for many of the manifestations of *VHL* loss of function. For example, HIFα deregulation appears to play a causal role in VHL-defective

ccRCC and in VHL-defective HB (1). Nonetheless, a number of other biochemical functions have been ascribed to pVHL, including binding to fibronectin, collagen, atypical PKC, and AKT (2-6). Different *VHL* germline mutations cause different organ-specific cancer risks in VHL disease (1). Type 1 VHL disease is defined as ccRCC and HB with low risk of PCC/PGL and is associated with disruptive mutations and gross deletions in *VHL* leading to very high HIFα expression. Type 2, which is predominantly associated with *VHL* missense mutations, is defined by the occurrence of PCC/PGL, either alone (type 2C) or in combination with hemangioblastomas (type 2A) or with hemangioblastomas and RCCs (type 2B). Some Type 2C mutants retain the ability to suppress HIFα (7, 8). This suggest that PCC/PGL in type 2C VHL disease are not caused by HIFα activation and thus VHL type 2C mutants would be a powerful tool to identify HIFα-independent VHL functions.

We previously reported that genetic alterations, including *VHL* alterations, linked to familial PCC/PGL may act by decreasing the activity of a 2-oxoglutarate-dependent oxygenase, EglN3, thereby reducing apoptosis of neural crest cells during development (9). Furthermore, EglN3-induced apoptosis requires its hydroxylase activity, but is independent of its role in suppressing HIFα (9). Using an unbiased genome-wide shRNA screen we identified the candidate 1p36 tumor suppressor KIF1Bβ, which is required for EglN3-dependent apoptosis and we and others identified loss-of-function germline *KIF1Bβ* mutations in subsets of PCC/PGL and neuroblastomas (10-12). However, EglN3 does not appear to hydroxylate KIF1Bβ, which led us to search for EglN3

pro-apoptotic substrates. Here we identified the pro-apoptotic BH3-only protein BIM-EL as a direct EglN3 hydroxylation substrate. BIM-EL represents an isoform of the *BCL2L11* gene. The three major BIM isoforms are BIM-EL, BIM-L and BIM-S and all contain a BH3 domain, but have different pro-apoptotic potencies. We found hydroxylation of BIM-EL, but not BIM-L and BIM-S, enables direct VHL binding, that masks the phosphorylation site that is critical for BIM-EL protein degradation. Importantly, VHL recognition of hydroxylated BIM-EL is abolished by *VHL* type 2C mutations, including type 2C mutations that do not result in HIFα stabilization. Furthermore, reintroduction of wild-type VHL, but not type 2C VHL mutants, into *VHL-/-* cells restores the ability of EglN3 to induce apoptosis. These studies suggest that PCC/PGLs linked to *VHL* mutations are caused by defects in EglN3-induced apoptosis because of a failure to stabilize BIM-EL.

RESULTS

EglN3-induced apoptosis and regulation of BIM-EL is hydroxylation and VHL-dependent.

We previously demonstrated that EglN3 activity is required for apoptosis when sympathetic neurons are deprived of nerve growth factor (NGF) in vitro (9, 10). We also confirmed that the superior cervical ganglia (SCG), which are composed of such neurons, from post-natal day 1 (P1) mice lacking *EglN3* are enlarged compared to their wild-type littermates (Fig. 1A), in keeping with a prior study (13). The proapoptotic BCL-2 family member BIM-EL is critical for neuronal apoptosis (14) and hypoxia's ability to suppress apoptosis after NGF withdrawal

involves suppression of BIM-EL (15). Thus, we investigated if EglN3 hydroxylation activity can induce BIM-EL.

We observed that BIM-EL protein was dramatically reduced in *EglN3-/-* SCG and primary mouse embryonic fibroblasts (MEFs) compared to littermate control *EglN3+/+* SCG and MEFs, respectively (Fig. 1B,C) and in neuroblastoma cells in which *EglN3* was downregulated with shRNA (Fig. 1D). To understand if BIM-EL protein levels are regulated by EglN3 hydroxylation activity, we made adenoviruses encoding wild-type (WT) EglN3 or a catalytic-dead EglN3 mutant (H196A). BIM-EL levels were restored in *EglN3-/-* MEFs infected with Ad-EglN3-WT, but not Ad-EglN3-H196A (Fig. 1E). Thus, EglN3 hydroxylation activity regulates BIM-EL expression.

To investigate if this effect on BIM-EL was specific to EglN3 amongst the three EglN paralogs, we specifically silenced *EglN1*, *EglN2*, or *EglN3* in HeLa cervical carcinoma cells using siRNAs (Fig. 1F and SI Appendix, Fig. S2A). BIM-EL protein levels were reduced by silencing *EglN3*, and to a much lesser extent by *EGLN2*, but not by silencing *EGLN1*. Conversely, silencing *EglN1* caused the greatest effect on HIF1α, consistent with earlier studies (16), whereas silencing *EglN3* had no measureable effect on HIF1α, suggesting specificity of function within the EGLN family members.

We next overexpressed EglN3 in cell lines of sympathoadrenal (PC12, rat) (SI Appendix, Fig. S1A) or neuronal origins (U87, human) (Fig. 1G) using the adenovirus described above. In these cells, wild-type, but not catalytic-dead, EglN3, induced BIM-EL and apoptosis as measured by caspase 3 cleavage and

crystal violet staining. Moreover, the effect of EglN3 on BIM-EL was blocked under anoxic conditions and by the hydroxylase inhibitors DMOG and FG0041 in *EglN3* primary MEFs (Fig. 1H).

To address whether induction of BIM-EL is necessary for EglN3 to induce cell death, we silenced *BIM-EL* with two independent shRNA's in U87 cells (Fig. 1I) or using two independent siRNAs in PC12 cells (SI Appendix, Fig. S1B). Silencing *BIM-EL* protected against EglN3-induced apoptosis as measured by crystal violet staining, caspase 3 cleavage, and nuclear fragmentation.

Since we observed that BIM-EL protein abundance is dependent on EglN3 hydroxylase activity, we investigated if this observation is VHL-dependent. Cre-mediated deletion of *VHL* in MEFs homozygous for a floxed *VHL* allele robustly decreased BIM-EL protein levels (Fig. 2A), reminiscent of the loss of BIM-EL in *EglN3*-/- MEFs. Furthermore, reintroducing HA-VHL (WT) into *VHL*-deficient RCC cells (786-O) restored BIM-EL protein expression (Fig. 2B) unless *EglN3* was inactivated with an effective shRNA (Fig. 2C) or by anoxia (Fig. 2D).

Type 2C VHL mutants predispose to PCC/PGL without grossly deregulating HIFα (7). We therefore asked if *VHL* type 2C mutations are loss of function with respect to BIM-EL regulation and if this is reflected in *VHL* defective human PCC/PGL. Compared to wild-type HA-VHL, type 2C HA-VHL (L188V and R64P) were clearly defective with respect to BIM-EL induction when reintroduced into 786-O cells despite their ability to repress HIF2α (Fig. 2E). Moreover, *VHL-/-* 786-O cells were resistant to EglN3-induced apoptosis (Fig. 2F). Importantly, reintroduction of wild-type VHL, but not the type 2C VHL mutant L188V, rescued

the ability of EglN3 to induce apoptosis as measured by crystal violet staining and caspase 3 cleavage (Fig. 2F). Consistent with the data in Fig. 1I, silencing BIM-EL also prevented EglN3-induced apoptosis in the context of 786-O cells (Fig. 2G). EglN3 expression also caused some growth inhibition seen in crystal violet staining two weeks' post infection in *VHL-/-* and mutant cells, consistent with previous reports that EgLN3 can suppress cell proliferation (17, 18). Similarly to 786-O cells, *VHL* knockdown in rat PC12 pheochromocytoma cells decreased BIM-EL levels (Fig. 2H) and protected against EglN3 induced apoptosis (Fig 2I). Reintroduction of human HA-VHL WT however, but not VHL 2C-L188V, restored BIM-EL expression and EglN3 induced apoptosis, suggesting that EglN3's apoptotic function is linked to VHL type 2C PCC/PGL pathogenesis .

Thus, we assayed BIM-EL protein level in a panel of human primary PCC/PGL tumors that were sequenced for PCC/PGL-susceptibility genes, including *VHL*, and analyzed for 1p36 deletion (12). Normal human adrenal glands were included as controls (Fig. 2J and SI Appendix, Fig. S2B). We observed low BIM-EL expression only in the PCC/PGL tumors carrying *VHL* mutations and not in other PCC/PGL, supporting our cell culture findings that BIM-EL protein regulation is VHL-dependent.

EglN3 hydroxylates BIM-EL at the Proline$^{67/70}$ residues enabling interaction with wild-type VHL but not VHL type 2C-disease mutants.

To test whether prolyl-hydroxylation of BIM-EL by EglN3 is responsible for the VHL-dependent regulation of BIM-EL abundance, we first performed EglN3 binding studies with BIM-EL using glutathione *S*-transferase (GST) pull-down assays. GST-BIM-EL bound to ^{35}S-labeled EglN3 produced by *in vitro* translation (IVT), but not to ^{35}S-EglN1 or ^{35}S-EglN2 (Fig. 3A and SI Appendix, Fig. S3A). No interaction was observed between ^{35}S-EglN3 and GST-BIM-L, a shorter BIM variant missing 116 amino acids generated by alternative splicing (Fig. 3A, and SI Appendix, Fig. S3A). Thus, we investigated if BIM-EL could be hydroxylated by EglN3 and subsequently recognized by VHL. *In vitro* translated HA-BIM-EL and HA-BIM-L were HA-immunoprecipitated and used in EglN3 hydroxylation assays. HA-HIF1α was tested in parallel as a positive control. HA-BIM-EL and HIF1α but not HA-BIM-L, captured ^{35}S-labeled VHL after incubation with EglN3 (Fig. 3B), suggesting that EglN3 hydroxylates proline(s) within the amino acid region that is missing in BIM-L. EglN3 enzymatic activity was required for VHL binding, because BIM-EL subjected to hydroxylation reactions using EglN3 catalytic-dead mutant (H196A) failed to capture ^{35}S-VHL (SI Appendix, Fig. S3B). Furthermore, a pan-hydroxyproline antibody immunoprecipitated an apoptosis-defective HA-BIM-EL apoptotic variant (BIM-EL-ΔBH3) from 293 cells (the apoptotic-defective variant was used to allow stable expression) that exogenously EglN3 unless the EglN3 was catalytically inactive or the cells were treated with DMOG (Fig. 3C and SI Appendix, Fig. S3C).

Next, we generated different peptides within the 116-aa region within BIM-EL to narrow the EglN3-binding domain and potential hydroxylation site (Fig. 3D).

We observed ^{35}S-EglN3 binding to biotinylated BIM-EL peptide corresponding to residues 65–89 (BIM-EL 65-89), but not to BIM-EL peptide corresponding to residues 55–79 (SI Appendix, Fig. S3D). However, despite EglN3 binding, we could not detect binding of VHL to BIM-EL 65-89 after incubation with EglN3 (SI Appendix, Fig. S3E). This prompted us to generate a longer peptide (40 aa), corresponding to BIM-EL-residues 57–96. This longer biotinylated BIM-EL peptide captured ^{35}S-VHL after the EglN3 hydroxylation reaction, similar to that of the biotinylated HIF1α–peptide residues 556–575 (SI Appendix, Fig. S3E). Next, we tested if BIM-EL hydroxylation is a specific function of EglN3 amongst the EglN paralogs. Incubation of the BIM-EL-peptide-57-96 with EglN3, but not with EglN1 or EglN2, promoted the capture of ^{35}S-VHL (Fig. 3E), consistent with our earlier observations that regulation of BIM-EL abundance (Fig. 1F) and binding to BIM-EL (Fig. 3A) is a distinguishing feature of EglN3. In contrast, and as previously reported (19), the HIF1α peptide was hydroxylated *in vitro* by all three EglN family members (Fig. 3E). Hydroxylation of the BIM-EL-peptide-57-96 was confirmed by LC-MS/MS analysis (Fig. 3F and SI Appendix, Fig. S3F-I). MS confirmed that EglN3, but not the catalytic-dead mutant, hydroxylated proline 67 and proline 70 (Fig. 3F and SI Appendix, Fig. S3F). We detected mono-hydroxylated peptide on either proline 67 (SI Appendix, Fig. S3G) or proline 70 (SI Appendix, Fig. S3H) as well as di-hydroxylated peptides on proline 67 and 70 (Fig. 3F). In addition to proline hydroxylation, we detected oxidation of the biotin residue, which is a common artefact, in hydroxylation reactions containing wild-type EglN3 or catalytic-dead EglN3 (20). The detected intensity of each proline

hydroxylated peptide was quantified and normalized to the non-hydroxylated peptide (Fig. 3G). Peptides mono-hydroxylated on proline 67 or proline 70 co-eluted in the chromatography, which prevented us from quantifying the hydroxylation of either site individually. To understand the importance of mono- or di-hydroxylation of the respective proline residues for VHL binding, we synthesized BIM-EL-57-96 peptides with the proline to alanine substitutions: P60A, P63A, P66A, P67A, P70A, P67/70A, and P66/67/70A, and measured their hydroxylation by EglN3 using the ^{35}S-VHL capture assay (Fig. 3H). The P60A and P63A proline substitutions did not alter hydroxylation relative to the wild-type peptide. In contrast, the P66A, P67A and P70A substitutions significantly impaired ^{35}S-VHL capture and the triple substitutions P66/67/70A completely abolished ^{35}S-VHL recognition (Fig. 3H). It is possible that the mutated P67A peptide generates some substrate recognition for proline 66. Jumping to neighboring lower affinity sites has been previously observed in *in vitro* enzymatic assays of other posttranslational modifications (21). In a reciprocal experiment, we synthesized BIM-EL-57-96 peptides in which proline 67(P-OH-67), proline 70 (P-OH-70), or both (P-OH-67/70) were hydroxylated (Fig. 3I). As expected, all three hydroxylated peptides could, similar to hydroxylated HIF1α peptide (556–575), captured 35S-pVHL (Fig. 3J). In contrast, non-hydroxylated BIM-EL peptide (BIM-EL-WT) did not capture ^{35}S-pVHL.

Our finding that BIM-EL expression can be restored by wild-type VHL, but not type 2C VHL mutants (Fig. 2E), suggested that the latter cannot recognize hydroxylated BIM-EL. Indeed, type 2C VHL mutants bound to a hydroxylated

HIF1α peptide, but failed to bind hydroxylated BIM-EL peptide (P-OH-67/70) (Fig. 4A). Type 1 and type 2A/B VHL mutants also failed to recognize hydroxylated BIM-EL (Fig. 4A). We complimented these studies by expressing either wild-type HA-pVHL (WT) or the corresponding type 1or 2A/B/C VHL mutants in 786-O cells and performing pulldown assays with immobilized BIM-EL or HIF1α peptides. As expected, wild-type VHL bound to the di-hydroxy-BIM-EL peptide (P-OH-67/70), but not to a non-hydroxylated BIM-EL peptide or scrambled peptide (Fig. 4B). Consistent with our findings in Fig. 4A, the type 2C VHL mutants bound to the hydroxylated HIF1α peptide, but not the hydroxylated BIM-EL peptide, while the type 1 and type 2A/B were defective for both (Fig. 4C). Consistent with these findings, only wild-type VHL fully restored BIM-EL levels when introduced into 786-O cells (Fig. 4D). In contrast, but in keeping with prior studies, both type 2C VHL mutants suppressed HIFα (Fig. 4D).

VHL-mediated regulation of BIM-EL protein stability is dependent on EglN3 enzymatic activity.

VHL stabilizes BIM-EL in RCC cells, but the mechanism is unknown (22). Since we observed that VHL binds to hydroxylated BIM-EL, we asked if this physical association stabilizes BIM-EL despite VHL's well-established role as a component of an E3 ubiquitin ligase. The BIM-EL sites hydroxylated by EglN3 (P67 and P70) are near a critical serine residue (S69) that dictates BIM-EL proteasomal degradation upon ERK phosphorylation (23). Thus, we hypothesized that binding of VHL to hydroxy-P67/P70 masks the S69

phosphorylation site and thus prevents the proteasomal degradation of BIM-EL. First, we used the proteasome inhibitor MG132 to determine if the loss of BIM-EL in *EglN3*-KO (-/-) primary MEFs was due to proteasomal degradation. MG132 increased BIM-EL protein abundance in *EglN3*-KO (-/-) MEFs to the level of *EglN3* WT (+/+) MEFs (Fig. 5A). A HIF1α immunoblot served as a positive control to assure MG132 activity. Likewise, MG132 treatment of *VHL*-/- cells (786-O) restored BIM-EL levels (Fig. 5B), providing evidence that loss of either *EglN3* or *VHL* accelerates BIM-EL proteasomal degradation. Importantly, phosphorylation of BIM-EL on the critical Ser69 residue required for protein turnover was markedly increased in both *EglN3*-/- MEFs (Fig. 5C and SI Appendix, Fig. S4A) and *VHL-/-* MEFs (Fig. 5D and SI Appendix, Fig. S4B), consistent with the idea that EglN3 and VHL block Ser69 phosphorylation.

Next, we investigated if VHL interacts with endogenous BIM-EL in 786-O cells expressing HA-VHL(WT) and if this was dependent on EglN3. BIM-EL was readily detected in anti-HA immunoprecipitates of cells expressing HA-VHL unless EglN3 was downregulated with an effective shRNA (Fig. 5E). Furthermore, BIM-EL co-immunoprecipitated only with wild-type VHL, but not VHL type 2C mutant L188V (Fig. 5F). To test if VHL binding to hydroxylated BIM-EL might block Ser69 phosphorylation, we performed *in vitro* ERK kinase assays. ERK-kinase activity was first measured using a wild-type BIM-EL-peptide (WT) or a hydroxylated BIM-EL-peptide (BIM-EL-P-OH-67/70) as ERK substrates. Both peptides were similarly phosphorylated by ERK-kinase *in vitro* as measured by phospho-BIM-EL(Ser69) immunoblot analysis (Fig. 5G). However, preincubation

with GST-VHL prevented the hydroxylated BIM-EL peptide (P-OH-67/70) from being phosphorylated by ERK (Fig. 5H).

To ask if EglN3 and VHL stabilizes BIM-EL protein, we treated 786-O cells with the protein synthesis inhibitor cycloheximide. The half-life of BIM-EL was shorter in *VHL*-/- 786-O cells compared to wild-type VHL (Fig. 5I,J). Similarly, the half-life of BIM-EL was shorter in *EglN3*-KO MEFs, accompanied with increased phosphorylation on Ser69, compared to wild-type MEFs (Fig. 5K,L). These results demonstrate that VHL and EglN3 specifically stabilize BIM-EL in cells by preventing Ser69 phosphorylation. In accord with these data, we show that exogenous expression of the apoptosis-defective mutant of BIM-EL (HA-BIM-ELΔBH3) harboring the serine 69 to alanine substitution (S69A) was stabilized in 786-O cells in the absence of VHL (Fig. 5M). Furthermore, exogenous BIM-EL wild-type (HA-BIM-ELΔBH3) protein was stabilized in VHL null cells (786-O) that were treated with different ERK kinase inhibitors (Fig. 5N).

Thus, we conclude that binding of VHL to hydroxylated BIM-EL prevents BIM-EL-Ser69 phosphorylation and degron recognition and thus allows BIM-EL to escape from proteasomal degradation (SI Appendix, Fig. S4C).

Loss of *EglN3* or *VHL* causes cisplatin drug resistance.

BIM protein degradation has been linked to cisplatin resistance in cancer therapy (24). ccRCC cells derived from renal epithelial cells, which are normally cisplatinum sensitive, and yet ccRCC and other VHL-associated neoplasms are generally resistant to chemotherapy, including cisplatinum. Thus, we investigated if loss of *EglN3* or *VHL* can likewise contribute to cisplatin resistance.

Silencing of *EglN3* has been recently described in high grade glioma (25) and *VHL* loss is well characterized in ccRCC (1). Therefore, we explored cisplatin responsiveness in isogenic 786-O (*VHL+/+* and *VHL-/-*) ccRCC cells, in neuroblastoma cells (SK-N-FI) that express EglN3 and VHL, and in primary (JM3, JM2, KS1, KS4, KS8, G3) and permanent (U87) glioblastoma cell lines (GBM) in which *EglN3* mRNA levels were determined by RNA Seq (26). (Fig. 6A). We identified only one human primary GBM cell line (JM3) expressing EglN3. In addition, high EglN3 expression was observed in human mature astrocytes compared to normal other human tissues (SI Appendix, Fig. S5A) (24), while EglN3 expression in the remaining primary GBM cultures were either significantly lower or undetectable altogether (Fig. 6A). We assessed the response of JM3 (*EglN3*-positive) and KS4 (*EglN3*-negative) cells to address their response to cisplatin. Cisplatin treatment caused a robust induction of endogenous EGLN3 accompanied by the induction of BIM-EL and caspase 3 cleavage in JM3 cells, but not the KS4 cells (Fig. 6B). To understand if cisplatin resistance was caused by the lack of *EglN3* expression, we reintroduced EglN3 into KS4 cells using lentivirus encoding wild-type EglN3 or catalytic dead mutant (H196A). Stable re-introduction of EglN3 wild-type, but not mutant, caused a marked increase of BIM-EL protein in KS4 cells, that was further induced by cisplatin, leading to sensitization of these cells to cisplatin-induced apoptosis (Fig. 6C). Although catalytic-dead EglN3 failed to rescue BIM-EL protein expression in untreated cells, it did cause a modest induction of BIM-EL in the presence of cisplatin. The significance of this finding is not clear, but could reflect a hydroxylase-

independent function of EglN3 that is unmasked by cisplatin (Fig. 6C). Nonetheless, the cells expressing EglN3 catalytic-dead mutant remained resistant to cisplatin induced apoptosis (Fig. 6C).

Similarly, lowering EglN3 levels in JM3 cells (SI Appendix, Fig. S5B) or SK-N-FI cells (SI Appendix, Fig. S5C) with an effective shRNA lowered BIM-EL levels and conferred cisplatin resistance (SI Appendix, Fig. S5C). Furthermore, reintroducing HA-VHL into *VHL-/-* 786-O cells restored the ability of cisplatin to induce BIM-EL and apoptosis in these cells (Fig. 6D).

Next, we tested if EglN3-null or VHL-null cells can be sensitized to cisplatin -induced apoptosis in combination with ERK inhibitors. BIM-EL expression was restored to that of EglN3 wild-type expressing KS4 glioma cells 24 hrs after treatment with various ERK inhibitors (SI Appendix, Fig. S5D). Despite BIM-EL induction in EglN3-null or EglN3-H196A mutant cells, ERK inhibitor alone caused only significant apoptosis in EglN3 wild-type (WT) expressing cells (Fig. 6E,F). Combined treatment of cisplatin and ERK inhibitor caused apoptosis irrespective of EglN3 status (Fig. 6E,F) without showing any further increase of BIM-EL protein compared to ERK inhibitor alone. Similarly, treatment of VHL null cells with an ERK inhibitor alone did not cause apoptosis, despite BIM-EL induction (Fig. 6G,H), but did so when combined with cisplatin (Fig. 6G and SI Appendix, Fig. S5E). Thus, highly efficient killing by the BIM-EL induced by ERK inhibitors in cells lacking EglN3 or VHL requires one or more collateral signals that can be provided by cisplatin.

DISCUSSION

The canonical function of VHL is to ubiquitinate hydroxylated HIFα for proteasomal degradation. HIFα deregulation can cause PCC and PGL, as evidenced by gain of function HIF2α and loss of function EglN1 mutations in rare familial cases. However, the mechanisms underlying the complex genotype–phenotype correlations in VHL disease cannot be explained by HIFα regulation. VHL type 2C mutations are not related to HIFα activation and preserve their ability to downregulate HIFα (7, 8). Here we identified a novel oxygen sensitive function of pVHL that is abolished by *VHL* type 2C mutations. We identified BIM-EL as a direct EglN3 hydroxylation substrate and that hydroxylated BIM-EL is bound and stabilized by binding to VHL, but not by VHL type 2C mutants. BIM-EL hydroxylation on P67 and P70 is in near proximity to the critical serine 69, which dictates BIM-EL proteasomal degradation upon ERK phosphorylation (23). We observed that pVHL binds to hydroxylated BIM-EL at P67/P70 and prevents ERK phosphorylation on serine 69, leading to BIM-EL protein stabilization. Indeed, low BIM-EL expression in the PCC/PGL tumors carrying *VHL* mutations confirms that BIM-EL protein regulation is VHL-dependent.

We previously reported that EGLN3 hydroxylase activity is linked to PCC pathogenesis through regulation of apoptosis during sympatho-adrenal development, which is independent of HIFα hydroxylation (9). Here we identified that VHL loss causes resistance to EGLN3-induced apoptosis and that this can be restored by wildtype VHL, but not by VHL type 2C mutants. Furthermore, we

found that EGLN3-induced apoptosis requires hydroxylation of BIM-EL, which in turn allows for VHL recognition of the protein, thus leading to BIM-EL protein stabilization. *Bim* deletion has been reported to cause protection against developmental and induced neuronal apoptosis, in both, central and peripheral neuron populations (14). Furthermore, inhibition of NGF deprivation–induced death by low oxygen levels during sympathetic neuronal development involves suppression of BIM-EL (15). By identifying BIM-EL as a direct EGLN3 hydroxylation substrate, we provide the missing mechanistic link between VHL type 2C PCC-mutations, EGLN3 hydroxylase activity, and escape from apoptosis during sympatho-adrenal development.

Thus, our work provides insights as for why VHL type 2C mutations contribute to PCC/PGL pathogenesis. We identified a biochemical activity that is lost by Type 2C pVHL mutants, leading to a loss of BIM-EL. Moreover, this biochemical activity affects neuronal apoptosis after NGF withdrawal, as do many of the other PCC/PGL-associated genes. Therefore, the law of parsimony suggests that dysregulation of BIM-EL contributes to the pathogenesis of PGLs caused by VHL mutations (including Type 2C mutations). Nonetheless, Type 2C mutants have also been shown to be defective with respect to other biochemical properties, including fibronectin and collagen binding (2-4). It is possible that these other biochemical properties are relevant to PGL as well.

Why germline type 1 VHL mutation (deleterious mutants) seldom causes PCC/PGL despite BIM-EL reduction has not been addressed in this work. However, we predict that complete loss of VHL during sympathoadrenal

development is not tolerated and thus does not result in PCC/PGL outcome. This argument is in line with observations in VHL conditional knockout studies in mice (TH-cre) which show that loss of VHL during development results in the disappearance of catecholaminergic cells (27), in contrast to conditional TH-EglN1^{KO} mice that causes hyperplasia in the carotid body (28). This suggests that unknown VHL functions are required for the formation of the sympathoadrenal cell lineage and therefore complete loss of VHL (type 1) might not be permissive in PCC/PGL pathogenesis. In contrast, in missense mutated VHL cells, reduction of BIM-EL protein might not impair the formation of the sympathoadrenal lineage. Instead it provides a mechanism to escape developmental apoptosis independent of HIFα regulation contributing to PCC/PGL. Our observation that all VHL mutated PCC/PGL tumors show reduced BIM-EL expression in contrast to other non VHL mutated PCC/PGL tumors support this. However, that would not exclude other VHL substrates contributing to VHL related pheochromocytoma.

Evading apoptosis is a hallmark of cancer. Every *VHL* mutation we have examined to date, whether type 1 and type 2, leads to loss of BIM-EL. It is therefore likely that loss of BIM-EL contributes to the pathogenesis of VHL-related neoplasms other than paragangliomas, including ccRCC and hemangioblastoma, as well as their characteristic insensitivity to chemotherapy. In this regard, cisplatinum damages renal epithelial cells, leading to renal dysfunction, and yet is inactive against ccRCCs. We showed that loss of VHL,

and subsequent downregulation of BIM-EL, renders ccRCC cells insensitive to cisplatinum. Thus, we investigated further EglN3 role during cisplatinum response. Cisplatin treatment induced EGLN3 in VHL WT expressing cells, accompanied by BIM-EL induction and apoptosis, whereas *EglN3*-silenced neuroblastoma cells or *VHL*-null ccRCC cells were resistant. Re-introduction of wild type VHL, but not by type 2C VHL mutants in ccRCC cells restored sensitivity. We also studied resistance to cisplatin in high grade glioma cells, since *EglN3* has been reported to be silenced during glioma progression (25). We observed that *EglN3*-silenced glioblastoma cells were cisplatin resistant, but sensitized upon re-introduction of wild-type EGLN3. In line with our observations, other studies also reported that EglN3 and BIM-EL are required for successful pro-apoptotic activity of various DNA damage–inducing chemotherapeutical agents (29, 30). By unraveling the precise molecular mechanism of BIM-EL stabilization by VHL and EglN3, we provide further insights into the chemoresistance that is typical of tumors lacking VHL or oxygen. Thus, restoration of BIM-EL protein expression by combination therapy using ERK inhibitors together with cisplatin might provide a promising approach for cancer therapy (SI Appendix, Fig. S5F).

Methods

Cell culture

Human neuroblastoma cell line SK-N-FI and the rat pheochromocytoma cell line

PC12 were maintained as previously described (10). Human glioblastoma cell line U87 was maintained in DMEM (glucose 1g/L) containing 10% fetal bovine serum (FBS). Mouse embryonic fibroblasts (MEFs) and human RCC cell line (786-O) were cultured in DMEM (glucose 4,5g/L) containing 10% fetal bovine serum (FBS) in 5% CO_2 at 37°C. The 786-0, SK-N-FI and PC12 cell lines were purchased from the American Tissue Culture Collection. *VHLfl/fl* immortalized MEF's have been previously described (31), containing a blasticidin resistance cassette and directed the expression of large T antigen K1 (K1 T antigen inactivate p53 but not pRB). Human primary glioblastoma cell cultures were established as previously described (26).

EglN3 knockout mice

Generation of the *EglN3* mouse strain is described in (10). P1 Super cervical ganglia dissections of EglN3 pups are described in (32).

Human tissue specimen

PCC and abdominal PGL were collected from patients operated and diagnosed at the Karolinska University Hospital, Stockholm, Sweden, previously characterized for mutations in 14 proposed PCC/PGL susceptibility genes (12) (SI Appendix, Fig. S2). Four histologically confirmed normal adrenal glands from de-identified patients were included as controls. VHL mutations in sample 21, 25, 96 and 108 have been previously described (12):

Sample 21: Diagnosed with cerebellar hemangioblastoma and

pheochromocytoma the same year. Syndromic VHL patient with a germline VHL mutation c.217C>T p.Gln73X (frameshift mutation resulting in truncated VHL , type 1). Please note: #21 has a truncating mutation. The risk of developing PCC in VHL type 1 patients is not zero, but lower than for type 2 patients.

Sample 25: Diagnosed with PCC at age of 13 with normal epinephrine and norepinephrine levels with no evidence of metastasis or relapse and no additional tumors. Syndromic VHL patient with a germline VHL mutation: c.193T>G p.Ser65Ala, pos 3:10183724.

Sample 96: Pheochromocytoma, trichoepithelioma eight years earlier (benign skin lesion). Apparently sporadic patient (no VHL syndrome) with a somatic VHL mutation. Mutations identified in sample 21: EGLN1 c.799G>A p.Glu267Lys + SDHA c.223C>T p.Arg75X + VHL c.386T>C p.Leu129Pro

Sample 108: Paraganglioma in 1998, basal cell carcinoma of the skin in 2013, follicular lymphoma in 2018. Apparently sporadic patient (no VHL syndrome) with a somatic VHL mutation: VHL c.593T>G p.Leu198Arg.

Ethical Considerations

Human samples (normal tissues, PCCs and PGLs) are covered both by an existing ethical approval (Drn 01-136, KI forskningsetikkommitté Nord). Human glioblastoma tissue specimens were collected via surgical resection under the ethical permit KI 2013/576-31, issued by the Ethical Review Board at Karolinska Institutet, in accordance with the declaration of Helsinki. All samples were obtained following an informed patient consent. Ethical permits for animal studies

were approved by the appropriate local and national authorities – Jordbruksverket, Sweden.

Peptide pull-down assay

Streptavidin beads were incubated with biotinylated peptides (synthesized by peptides&elephants GmbH) and rotated for 1hour at room temperature. ^{35}S-VHL produced by IVT was captured as previously described (9). For pull down assays using VHL-expressing 786-O cells, conjugated streptavidin beads with biotinylated peptides were incubated with 786-0 cell lysate overnight at 4°C with rotation. Samples were then washed 4 times with immunoprecipitation wash buffer (0.5% NP-40, 150mM NaCl, 10mM Tris-HCl) and eluted with 30ul Laemmli buffer, boiled for 5 minutes and centrifuged at 8000xg for 30 seconds. Eluted supernatant was subjected to immunoblot analysis.

Peptide hydroxylation and ^{35}S-VHL binding assay

FLAG-EGLN1/2/3 and VHL were produced by *in vitro* transcription /translation reactions (IVT) using TnT® T7 Quick Master Mix. 1ug BIM-EL and HIF1α biotinylated peptides were respectively conjugated with Streptavidin agarose beads in 1ml PBS at room temperature with rotation for 1h. The beads pellet was washed twice with PBS and once with hydroxylation buffer (40mM HEPES, ph7.4, 80mM KCl). The pellet was resuspended with 300ul hydroxylation reaction buffer supplemented with 100uM FeCL2, 2mM Ascorbate and 5mM 2-oxolgutarate. 15ul IVT-synthesized EGLN was added to start the hydroxylation.

The hydroxylation reaction was processed for 2 hours at room temperature with rotation. 500ul EBC buffer was added to the reaction buffer to stop the hydroxylation and subsequently, 15ul IVT-synthesized S35 radioactive labeled VHL was added and this mixture was incubated overnight. Samples were centrifuged at 8000xg for 30 seconds and washed five times with wash buffer (0.5% NP-40, 150mM NaCl, 10mM Tris-HCl). Bound protein complexes were eluted with 30ul Laemmli buffer, boiled for 5 minutes and centrifuged at 8000xg for 30 seconds. Eluted supernatant was analyzed by immunoblot.

Full length BIM-EL hydroxylation and S^{35}VHL capture

EglN3 WT, EglN3 mutant, ^{35}S-VHL, BIM-EL were produced by *in vitro* transcription /translation reactions using TnT® T7 Quick Master Mix. *In vitro* translated BIM-EL was added to 300ul hydroxylation reaction buffer supplemented with 100uM FeCL2, 2mM Ascorbate and 5mM 2-oxolgutarate. 15ul unprogrammed reticulocyte lysate, IVT-synthesized wild-type EglN3 or EglN3 mutant were added to start the hydroxylation. The hydroxylation reaction was processed for 2 hours at room temperature with rotation. 500ul EBC buffer was added to the reaction buffer to stop the hydroxylation. 15ul IVT-synthesized ^{35}S-VHL was added and this mixture was incubated for 2 hours at room temperature with rotation. BIM-EL was immunoprecipitated with anti-BIM-EL antibody overnight at 4°C with rotation and captured with protein G beads. The beads pellet was then washed five times with immunoprecipitation wash buffer (0.5% NP-40, 150mM NaCl, 10mM Tris-HCl). Bound protein complexes were

eluted with 30ul Laemmli buffer, boiled for 5 minutes and centrifuged at 8000xg for 30 seconds. Eluted supernatant was analyzed by immunoblot or S^{35} autoradiography.

Peptide hydroxylation assay and mass spectrometry analysis

The hydroxylation assay with BIM-EL peptide was performed as described above. After hydroxylation, BIM-EL peptide conjugated beads were washed one time with hydroxylation buffer and three times with IP buffer without detergent. Samples were processed as described in (20). Biotinylated peptides were digested with chymotrypsin and directly analyzed by MS. Peptides were analyzed on a Q-Exactive mass spectrometer connected to an Ultimate Ultra3000 chromatography system incorporating an autosampler (both Thermo Scientific). Proteolytic or synthesized peptides for each sample (5 µL) were applied to a home-made column (250-mm length, 75-µm inside diameter) (packed with 1.8 µm UChrom C18) and separated using a 40-min reverse-phase acetonitrile gradient [5–70% (vol/vol) acetonitrile] with a 250-nL/min flow rate. The mass spectrometer was operated in positive ion mode with a capillary temperature of 220 °C and a 2000 V potential applied to the column. Variable modifications were N-terminal biotin, N-terminal biotin hydroxylation and proline hydroxylation.

Hydroxyproline Immunoprecipitation

293FT cells were transfected with Flag-EglN3 and HA-BIM-EL apoptotic dead mutant (∆BH3). 40 hours after transfection, cells were treated with MG132 and/or

DMOG for 8hours as indicated. Cells were washed once in ice-cold PBS, lysed with EBC buffer (50mM Tris at pH 8.0, 120mM NaCl, 0.5% NP-40) containing protease inhibitors. Lysate was centrifuged at 14,000 × *g* for 20 minutes to remove cellular debris and the resulting supernatant was incubated with anti-Hydroxyproline antibody (Abcam ab37067, batch: GR3215743-1) with overnight at 4°C. Samples were incubated for 4 hours with rotation at 4°C with 30ul Protein G agarose beads (sc-2002, SANTA CRUZ) (50% slurry) pre-washed twice with immunoprecipitation wash buffer (0.5% NP-40, 150mM NaCl, 10mM Tris-HCl). Samples were centrifuged at 8000xg for 30 seconds and washed five times with wash buffer (0.5% NP-40, 150mM NaCl, 10mM Tris-HCl). Bound protein complexes were eluted with 30ul Laemmli buffer, boiled for 5 minutes and centrifuged at 8000xg for 30 seconds. Eluted supernatant was analyzed by BIM-EL immunoblot.

Expression Plasmids, shRNA and siRNA's

pcDNA3 Flag-EglN3, Flag-H196A-mutant and pcDNA3-VHL including *VHL*-missense mutations are described previously (9). pcDNA3 HA-BIM-EL (mouse) and pcDNA3 HA-BIM-EL apoptotic mutant (ratBIM-EL∆BH3) were kind gifts from Stanley J. Korsmeyer, Dana-Farber Cancer Institute, USA. ratBIM-EL∆BH3 was a mutation in the BH3 domain: L^{150}RRIGDEFN^{158} mutated to A^{150}RRIAAEFN^{158}. Amino acid numbering refers to the rat Bim-EL sequence. ratBIM-EL∆BH3_S65A mutant was made using a site-directed mutagenesis kit (Aligent). Rat BIM-EL serine 65 residue correspond to human BIM-EL serine 69

residue. GST-BIM-EL and GST-BIM-L were kind gifts from S. Cook lab, Babraham Institute, Cambridge, UK. Lentivirus encoding FLAG-EglN3 and FLAG-EglN3-H196A was generated in 293FT cells as previously described (10). siRNAs targeting EglN1, EglN2 or EglN3 have been previously described and validated (34). Lentivirus encoding shRNAs targeting *BIM* and *EglN3* were generated using the pLKO.1 plasmid using the following sequences: human BIM-EL#54 5'-CCGGAGCCGAAGACCACCCACGAATCTCGAGATTCGTGGGTGGTCTTCGGCTTTTTT-3'; human BIM-EL#77 5'-CCGGGACCACCCACGAATGGTTATCCTCGAGGATAACCATTCGTGGGTGGTCTTTTTG-3'; human EglN3 5'-CCGGGTTCTTCTGGTCAGATCGTAGCTCGAGCTACGATCTGACCAGAAGAACTTTTTG-3'.

P-ERK kinase activity assay

1ug biotinylated hydroxylated BIM-EL-peptides were conjugated with Streptavidin agarose beads in 1ml PBS at room temperature with rotation for 1h. The beads pellet was washed three times with PBS and resuspended with 500ul PBS supplemented with 1ug purified GST-VHL protein for 2 hours at room temperature. Samples were centrifuged at 8000xg for 30 seconds and washed three times with PBS and re-suspended with 40ul ADBI (assay dilution buffer i) (20mM MOPS, ph7.2, 25mM beta-glycerol phosphate, 5mM EGTA, 1mM sodium orthovanadate, 1mM dithiothreitol) supplemented with 10ul Mg^{2+}/ATP cocktail (75mM magnesium chloride and 500uM ATP in ADBI) and 200ng purified P-ERK

(14-173 Merck Millipore). The phosphorylation assay (MAP Kinase/Erk Assay, non-radioactive, 17-191 Merck Millipore) was processed for 30 minutes at room temperature with rotation at 30°C. Samples were centrifuged at 8000xg for 30 seconds and washed three times with PBS and eluted with 30ul Laemmli buffer, boiled for 5 minutes and centrifuged at 8000xg for 30 seconds. Eluted supernatant was analyzed by immunoblot using phosphor specific BIM antibody (p-Ser69 (D7E11).

BIM-EL Half-life

786-0 cells were cultured in 6-well plates in 2 ml DMEM medium to reach 50% confluency. Cells were treated with 10 uM cyclohexamide at the indicated times, harvested and lysed in 150ul EBC lysis buffer. Lysates were analyzed by immunoblotting with rabbit anti-BIM-EL antibody. Image J Densitometry analysis was performed to quantify BIM-EL expression and determine protein half-life.

Statistics

Statistical analyses were performed when appropriate and *P* values indicated by an asterisk in the figure legends. Significant differences between means for multiple comparison analyses were conducted using ANOVA, followed by Bonferroni correction for post hoc analysis.

REFERENCES

1. Kaelin WG, Jr. (2008) The von Hippel-Lindau tumour suppressor protein: O2 sensing and cancer. *Nature reviews* 8(11):865-873.
2. Kurban G*, et al.* (2008) Collagen matrix assembly is driven by the interaction of von Hippel-Lindau tumor suppressor protein with hydroxylated collagen IV alpha 2. *Oncogene* 27(7):1004-1012.
3. Grosfeld A*, et al.* (2007) Interaction of hydroxylated collagen IV with the von hippel-lindau tumor suppressor. *The Journal of biological chemistry* 282(18):13264-13269.
4. Ohh M*, et al.* (1998) The von Hippel-Lindau tumor suppressor protein is required for proper assembly of an extracellular fibronectin matrix. *Mol Cell* 1(7):959-968.
5. Okuda H*, et al.* (1999) Direct interaction of the beta-domain of VHL tumor suppressor protein with the regulatory domain of atypical PKC isotypes. *Biochemical and biophysical research communications* 263(2):491-497.
6. Guo J*, et al.* (2016) pVHL suppresses kinase activity of Akt in a proline-hydroxylation-dependent manner. *Science* 353(6302):929-932.
7. Hoffman MA*, et al.* (2001) von Hippel-Lindau protein mutants linked to type 2C VHL disease preserve the ability to downregulate HIF. *Human molecular genetics* 10(10):1019-1027.
8. Clifford SC*, et al.* (2001) Contrasting effects on HIF-1alpha regulation by disease-causing pVHL mutations correlate with patterns of tumourigenesis in von Hippel-Lindau disease. *Human molecular genetics* 10(10):1029-1038.
9. Lee S*, et al.* (2005) Neuronal apoptosis linked to EglN3 prolyl hydroxylase and familial pheochromocytoma genes: developmental culling and cancer. *Cancer Cell* 8(2):155-167.
10. Schlisio S*, et al.* (2008) The kinesin KIF1Bbeta acts downstream from EglN3 to induce apoptosis and is a potential 1p36 tumor suppressor. *Genes & development* 22(7):884-893.
11. Yeh IT*, et al.* (2008) A germline mutation of the KIF1Bβ gene on 1p36 in a family with neural and nonneural tumors. *Human genetics* 124(3):279-285.
12. Welander J*, et al.* (2014) Rare germline mutations identified by targeted next-generation sequencing of susceptibility genes in pheochromocytoma and paraganglioma. *The Journal of clinical endocrinology and metabolism*:jc20134375.
13. Bishop T*, et al.* (2008) Abnormal sympathoadrenal development and systemic hypotension in PHD3-/- mice. *Molecular and cellular biology* 28(10):3386-3400.
14. Putcha GV*, et al.* (2001) Induction of BIM, a proapoptotic BH3-only BCL-2 family member, is critical for neuronal apoptosis. *Neuron* 29(3):615-628.
15. Xie L, Johnson RS, & Freeman RS (2005) Inhibition of NGF deprivation-induced death by low oxygen involves suppression of BIMEL and activation of HIF-1. *The Journal of cell biology* 168(6):911-920.
16. Berra E*, et al.* (2003) HIF prolyl-hydroxylase 2 is the key oxygen sensor setting low steady-state levels of HIF-1alpha in normoxia. *EMBO J* 22(16):4082-4090.
17. Henze A-T*, et al.* (2014) Loss of PHD3 allows tumours to overcome hypoxic growth inhibition and sustain proliferation through EGFR. *Nature Communications* 5:5582.
18. Hogel H, Rantanen K, Jokilehto T, Grenman R, & Jaakkola PM (2011) Prolyl hydroxylase PHD3 enhances the hypoxic survival and G1 to S transition of carcinoma cells. *PLoS One* 6(11):e27112.
19. Kaelin WG, Jr. & Ratcliffe PJ (2008) Oxygen sensing by metazoans: the central role of the HIF hydroxylase pathway. *Mol Cell* 30(4):393-402.
20. Rodriguez J*, et al.* (2016) Substrate-Trapped Interactors of PHD3 and FIH Cluster in Distinct Signaling Pathways. *Cell Rep* 14(11):2745-2760.
21. Treier M, Staszewski LM, & Bohmann D (1994) Ubiquitin-dependent c-Jun degradation in vivo is mediated by the delta domain. *Cell* 78(5):787-798.
22. Guo Y, Schoell MC, & Freeman RS (2009) The von Hippel-Lindau protein sensitizes renal carcinoma cells to apoptotic stimuli through stabilization of BIM(EL). *Oncogene* 28(16):1864-1874.
23. Luciano F*, et al.* (2003) Phosphorylation of Bim-EL by Erk1/2 on serine 69 promotes its degradation via the proteasome pathway and regulates its proapoptotic function. *Oncogene* 22(43):6785-6793.

24. Wang J, Zhou JY, & Wu GS (2011) Bim protein degradation contributes to cisplatin resistance. *The Journal of biological chemistry* 286(25):22384-22392.
25. Henze AT*, et al.* (2014) Loss of PHD3 allows tumours to overcome hypoxic growth inhibition and sustain proliferation through EGFR. *Nat Commun* 5:5582.
26. Kurtsdotter I*, et al.* (2017) SOX5/6/21 Prevent Oncogene-Driven Transformation of Brain Stem Cells. *Cancer research* 77(18):4985-4997.
27. Macias D, Fernandez-Aguera MC, Bonilla-Henao V, & Lopez-Barneo J (2014) Deletion of the von Hippel-Lindau gene causes sympathoadrenal cell death and impairs chemoreceptor-mediated adaptation to hypoxia. *EMBO Mol Med* 6(12):1577-1592.
28. Fielding JW*, et al.* (2018) PHD2 inactivation in Type I cells drives HIF-2alpha-dependent multilineage hyperplasia and the formation of paraganglioma-like carotid bodies. *J Physiol*.
29. Delbridge AR*, et al.* (2016) RAG-induced DNA lesions activate proapoptotic BIM to suppress lymphomagenesis in p53-deficient mice. *J Exp Med* 213(10):2039-2048.
30. Xie L*, et al.* (2012) PHD3-dependent hydroxylation of HCLK2 promotes the DNA damage response. *J Clin Invest* 122(8):2827-2836.
31. Young AP*, et al.* (2008) VHL loss actuates a HIF-independent senescence programme mediated by Rb and p400. *Nature cell biology* 10(3):361-369.
32. Fell SM*, et al.* (2017) Neuroblast differentiation during development and in neuroblastoma requires KIF1Bbeta-mediated transport of TRKA. *Genes & development* 31(10):1036-1053.
33. Li S*, et al.* (2016) The 1p36 Tumor Suppressor KIF 1Bbeta Is Required for Calcineurin Activation, Controlling Mitochondrial Fission and Apoptosis. *Dev Cell* 36(2):164-178.
34. Zhang Q*, et al.* (2009) Control of Cyclin D1 and Breast Tumorigenesis by the EglN2 Prolyl Hydroxylase. *Cancer Cell* 16(5):413-424.

FIGURE LEGENDS

Figure 1. EgIN3 regulation of BIM-EL protein is hydroxylation dependent.

(A) Photographs of dissected mouse superior cervical ganglia (SCG) of the indicated genotype and age. **(B)** Anti-BIM-EL immunoblot of dissected superior cervical ganglion (SCG) from 1 week old mice of the indicated genotype. **(C)** Anti-BIM-EL immunoblot of primary EgIN3-MEFs of indicated genotype. **(D)** Anti-BIM-EL immunoblot of SK-N-FI cells that were stably transduced with lentivirus encoding shRNA targeting EgIN3 (shEgIN3) or scramble control (shSCR). **(E)** Immunoblot analysis of EgIN3-MEFs transduced with adenovirus encoding either wild-type EgIN3, catalytic-dead mutant (H196A) or GFP-control (GFP). **(F)** Anti-BIM-EL immunoblot analysis of HeLa cells transfected with siRNA targeting EgIN1, EgIN2, EgIN3 or non-targeting control (SCR) as indicated. **(G)** Immunoblot and crystal violet staining of U87 cells transduced with adenovirus encoding wild-type EgIN3, catalytic dead mutant (H196A) or GFP-control (Ctr). 48h post-adenovirus transduction, cells were supplemented with medium and maintained in culture for one additional week, followed by crystal violet staining. **(H)** Immunoblot of EgIN3 primary MEF's with indicated genotype upon normoxic or anoxic conditions for 16h or treated with 1mM DMOG or 50uM FG0041. **(I)** Left panel: Crystal violet staining of U87 cells stably transduced with lentiviral pLKO shRNA targeting BIM (shBIM) or non-targeting control (shSCR) and subsequently transiently transduced for 48 hrs with adenovirus encoding EgIN3 or GFP-control. The corresponding immunoblot is shown in the right panel.

Figure 2. BIM-EL protein regulation by EgIN3 is depending upon pVHL.

(A) Anti-BIM-EL immunoblot of *VHL*+/+ and *VHLfl/fl* MEFs (immortalized by K1 large T antigen) that were transiently transduced with adenovirus encoding cre-recombinase or GFP-control. **(B)** Anti-BIM-EL immunoblot analysis of 786-O VHL null cells (-/-) stably transfected to generate wild-type VHL (WT). **(C)** Immunoblot of 786-O cells with indicated VHL status transduced with lentiviral pLKO shRNA targeting EglN3 or non-targeting control (shSCR). **(D)** Immunoblot of 786-O WT-VHL (WT) and VHL null cells (-/-) under normoxic or anoxic conditions for 16h. **(E)** Immunoblot of 786-O cells stably transfected to generate the indicated VHL species. **(F)** Crystal violet staining (left) of 786-O cells with indicated VHL status. Cells were transiently transduced for 48hr with adenovirus encoding either wild-type EglN3 or GFP-control. Cells were maintained in culture for an additional week, before being subjected to crystal violet staining. The corresponding immunoblot (right) is shown 48h after infection. **(G)** Crystal violet staining and immunoblot of 786-O cells expressing HA-VHL that were stably transduced with lentiviral-encoded shRNA targeting BIM (sh*BIM*) or non-targeting control (shSCR). Cells were transiently transduced with adenovirus encoding EglN3 or GFP-control. **(H)** Immunoblot analysis of stable polyclonal PC12 cells expressing the indicated human VHL species. PC12 clones were transiently transduced for 72 hours with lentivirus encoding shRNA targeting endogenous ratVHL (sh-*rVHL*) or scramble control (sh-*SCR*). Note: *VHL* long term knockdown was not tolerated in PC12 cells. **(I)** Percentage of fragmented nuclei of stable PC12 clones 3 days after co-transfection to generate GFP-histone and Flag-EglN3 along with pLKO plasmid targeting rat*VHL* (sh-*rVHL*) or scramble control (shSCR). One way

ANOVA was used to determine the statistical significance using Prism software ****p<0.0001. **(J)** Anti-BIM-EL immunoblot analysis of human normal adrenal glands and human primary pheochromocytoma (PCC) and paraganglioma (PGL) tumors. VHL mutation and 1p36 status have been characterized as indicated.

Figure 3. BIM-EL is hydroxylated by EglN3 at Proline 67/70 causing pVHL recognition.

(A) Autoradiograms showing recovery of ^{35}S-labeled EglN1, EglN2, EglN3, proteins bound to GST-BIM-EL or GST-BIM-L fusion proteins (GST protein as a negative control). ^{35}S labeling was carried out by *in vitro* translation reaction with retic lysate (IVT). **(B)** Autoradiograms showing recovery of ^{35}S-labeled VHL protein bound to HA-immunoprecipitated full length BIM-EL, BIM-L or HIF1α that were first subjected before to hydroxylation by EglN3 wild-type (WT). IgG served as negative control. ^{35}S labeling was carried out by IVT with retic lysate. EglN3, BIM-EL, BIM-L or HIF1α were produced by cold IVT. Flag-EglN3 expression was verified by immunoblot (5% input). **(C)** Immunoprecipitation using anti-hydroxyproline antibody (a-HydroxyP) from 293T cells that were transiently transfected with plasmids encoding HA-BIM-EL apoptotic mutant (ΔBH3) and Flag-EglN3 wild-type (WT) or catalytic-dead mutant (Mut). Immunoblots showing co-immunoprecipitation of HA-BIM-EL-ΔBH3. **(D)** Schematic representation of the various biotinylated synthetic BIM-EL peptides used for the EglN3 binding and hydroxylation assays. **(E)** Autoradiograms showing recovery of ^{35}S-labeled VHL protein bound to biotinylated BIM-EL-peptide-57-96 or HIF1α peptide-556–

575. Prior to pull-down, peptides were incubated with either EglN1, EglN2, EglN3 or EglN3 catalytic mutant (Mut) generated by IVT or unprogrammed reticulocyte lysate (-). Expression of IVT-produced EglN proteins in each reaction was verified by immunoblot. **(F)** Mass spectrometry of biotinylated BIM-EL-peptide subjected to EglN3 hydroxylation assay. Representative fragmentation spectra of hydroxylated Biotin-HGSPQGPLAPP(ox)ASP(ox)GP. **(G)** Hydroxylation levels of proline residue 67 and 70 of BIM-EL peptide (mono- or double hydroxylation are indicated as mono-HyP and 2HyP) following hydroxylation with EglN3 wild-type (wt) or catalytic mutant generated via IVT. The detected intensity of each hydroxylated peptide was normalized to the non-hydroxylated peptide. **(H)** Autoradiograms of EglN3 hydroxylation and S35-VHL capture as shown in (E) using biotinylated BIM-EL peptides containing proline to alanine substitutions, or no substitution (WT). **(I)** A schematic illustration of synthetic biotinylated BIM-EL-peptides, unmodified (WT), or hydroxylated at P-OH-67, P-OH-70 and P-OH-67/70. **(J)** Autoradiograms showing recovery of ^{35}S-labeled VHL protein bound to biotinylated BIM-EL peptides with indicated hydroxyl-prolines as outlined in I. Synthetic biotinylated HIF1α peptide (residues 556–575) with hydroxylated proline 564 (HIF1α-P-OH) was included as a control. Unmodified peptide is indicated as BIM-EL-WT.

Figure 4. VHL disease mutations fail to recognize proline hydroxylated BIM-EL.

(A) Autoradiograms showing recovery of ^{35}S-labeled VHL protein (WT) or corresponding disease mutants (as indicated) bound to biotinylated BIM-EL-peptides synthesized with double hydroxyl-prolines on proline 67 and 70 (BIM-EL-P-OH-67/70). Synthetic biotinylated HIF1α peptide (residues 556–575) with hydroxylated proline 564 (HIF1α-P-OH) was included as a control. An un-programmed IVT was used as a negative control. **(B)** Immunoblot of HA-VHL pull-down using biotinylated BIM-EL-P-OH-67/70-peptide or unmodified BIM-EL peptide (WT) or control peptide (scramble) incubated with whole cell lysate from 786-O HA-VHL expressing cells. **(C)** Peptide pulldown as shown in (B) using either biotinylated BIM-EL-P-OH-67/70-peptide or biotinylated HIF1αP-OH peptide incubated with whole cell lysates from 786-O cells expressing either HA-VHL wild-type (WT) or HA-VHL disease mutants. **(D)** Immunoblot analysis of endogenous BIM-EL and HIF2α protein expression in 786-O cells expressing either HA-VHL wild-type (WT) or HA-VHL disease mutants.

Figure 5. VHL regulates BIM-EL protein stability depending on EglN3 enzymatic activity.

(A) Immunoblot of *EglN3*-MEFs with indicated genotype treated for 6h with proteasomal inhibitor MG132 (10uM) or DMSO. **(B)** Immunoblot of 786-O VHL null cells (-/-) or stably cells transfected to generate wild-type HA-VHL (WT) treated for 6h with proteasomal inhibitor MG132 (10uM) or DMSO as control. **(C)** Anti-phospho-BIM-EL(Ser69) immunoblot analysis of whole cell lysates from EglN3 MEFs with indicated genotype **(D)** Anti-phospho-BIM-EL(Ser69) immunoblot of whole cell lysates derived from VHL MEFs with indicated

genotype transduced with lentivirus encoding either cre-recombinase or empty control lentivirus. **(E)** HA-VHL immunoprecipitation from 786-O cells transduced with lentivirus encoding shRNA targeting EglN3 (shE3) or scramble control (SCR). Immunoblots showing co-immunoprecipitation of endogenous BIM-EL and HA-VHL expression. **(F)** HA-VHL immunoprecipitation from 786-O cells with stable expression of either HA-VHL wild-type (WT) or HA-VHL type 2C mutant (L188V). VHL-null cells (-/-) served as negative control. Immunoblots showing co-immunoprecipitation of endogenous BIM-EL and HA-VHL expression. **(G)** ERK-kinase activity measured by using wild-type BIM-EL-peptide (WT) or hydroxylated peptide BIM-EL-P-OH-67/70 as substrates. Peptides were incubated with purified active ERK as indicated and kinase activity was measured by phospho-BIM-EL(Ser69) immunoblot analysis. **(H)** ERK-kinase activity was measured as in (G) using hydroxylated BIM-EL-P-OH-67/70 peptide. Prior to ERK-kinase reaction, the peptide was incubated with purified GST-VHL as indicated. Shown is the immunoblot of phospho-BIM-EL(Ser69) peptide indicating that the presence of VHL prevent substrate recognition and phosphorylation by ERK. **(I)** 786-O VHL-null cells (-/-) or stable HA-VHL wild-type (WT) expressing cells were treated with 10μg/ml cycloheximide (CHX). At the indicated time points, whole-cell lysates were prepared for immunoblot analysis. **(J)** Quantification of the band intensities in (I). **(K)** EglN3 MEFs with indicated genotype were treated with cycloheximide (CHX) at the concentration of 10μg/ml and whole-cell lysates were prepared for immunoblot analysis at the indicated time points. **(L)** Quantification of the band intensities in (K). **(M)** Immunoblot of

786-O VHL-null (-/-) cells co-transfected with HA-VHL together with apoptotic defective HA-BIM-EL-ΔBH3 (indicated as "WT") or HA-BIM-EL-ΔBH3-S69A mutant. **(N)** Immunoblot of 786-0 VHL-/- cells that were transiently transfected with plasmids encoding apoptotic defective HA-BIM-EL-ΔBH3 and HA-VHL as indicated. 24 hrs after transfection, cells were respectively treated for 24 hrs with different ERK-kinase inhibitors SCH772984 (1uM), Ulixertinib (1uM), U0126 (10uM).

Figure 6. Loss of EglN3 or VHL contributes to Cisplatin drug resistance.

(A) Expression levels of EglN3, as represented by RPKM values, in human high-grade glioblastoma cells (JM3, JM2, KS1, KS4, KS8, G3) and human U87 glioma cell line. Data are shown as mean ±SEM. ***, $p<0.001$. **(B)** Crystal violet staining and immunoblot analysis of human glioblastoma cells JM3 (EglN3 positive) and KS4 (EglN3 negative) cells treated with Cisplatin (5uM) for 48h. For crystal violet staining, cells were maintained in culture for additional 5 days. Immunoblot analysis was performed 48h post-cisplatin treatment. **(C)** Crystal violet staining and immunoblot analysis of KS4 cells stably transduced with lentivirus encoding Flag-EglN3 wild-type (WT), catalytic dead mutant (H196A) or empty control. Stable clones were treated with cisplatin (5uM) as indicated. Immunoblot was performed 48h post-Cisplatin treatment. For crystal violet staining, cells were maintained for additional 5 days in culture. **(D)** Crystal violet staining and immunoblot analysis of 786-O cells with indicated VHL status. Cells were treated with cisplatin once (5uM). Immunoblot was performed 72h post-cisplatin

treatment. For crystal violet staining, cells were maintained in culture for additional 4 days. **(E-F)** Crystal violet staining of KS4 stably transduced cells as (C) and treated once with cisplatin (5uM), Erk inhibitor SCH772984 (SCH 5uM) or combination of these two drugs as indicated. For crystal violet staining, cells were maintained for one week. Corresponding immunoblot shown in (**F**) 48 hrs post treatment. **(G-H)** Crystal violet staining (**G**) and corresponding immunoblot (**H**) of stable 786-O cells treated once with cisplatin (5uM), ERK-inhibitor SCH772984 (SCH 1uM) or combination of both as indicated for 72 h. For crystal violet staining, cells were maintained for 7 days.

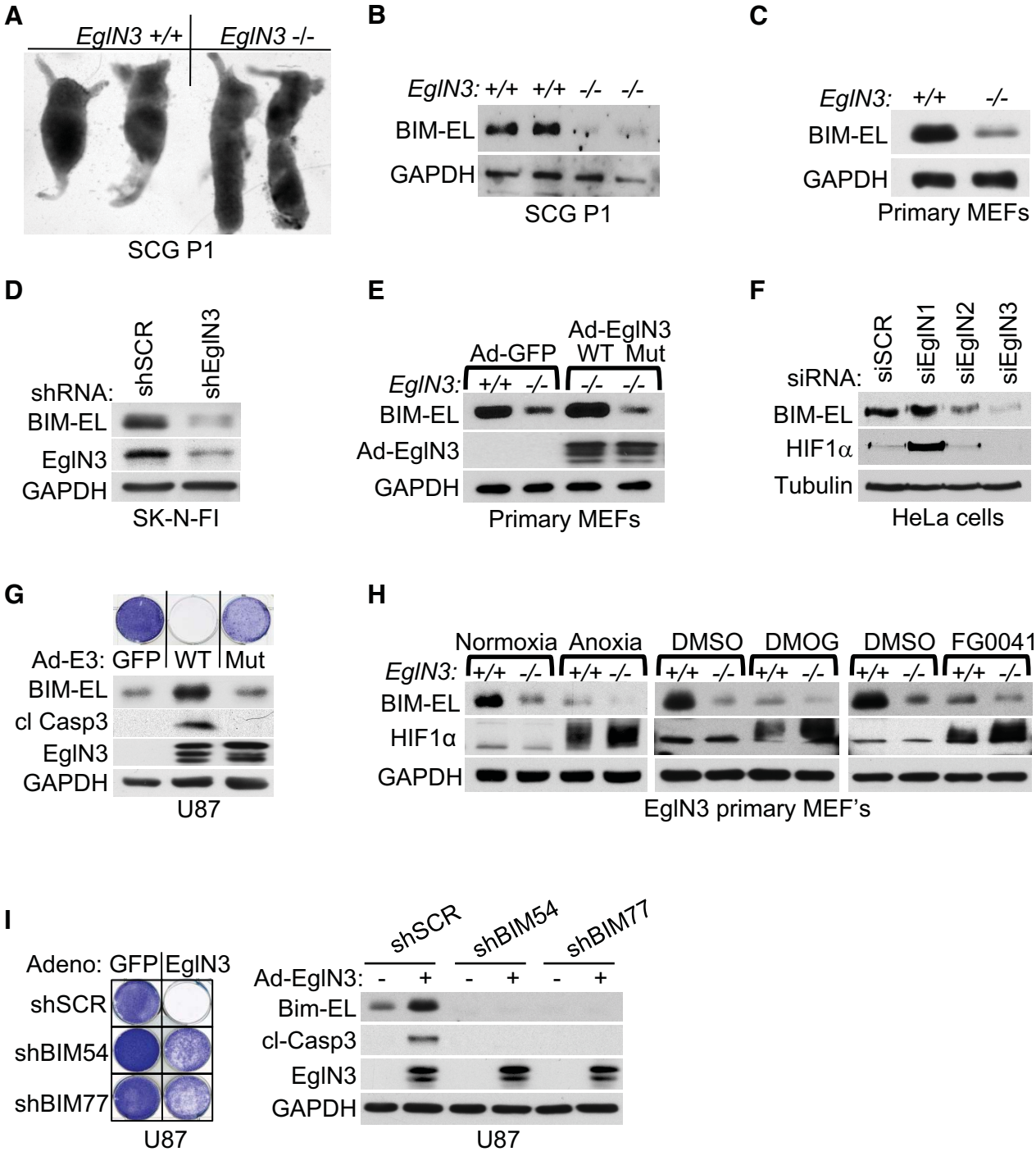
A
EgIN3 +/+
EgIN3 -/-
SCG P1
B
EgIN3: +/+ +/+ -/- -/-
BIM-EL
GAPDH
SCG P1
C
EgIN3: +/+ -/-
BIM-EL
GAPDH
Primary MEFs
D
shRNA: shSCR shEgIN3
BIM-EL
EgIN3
GAPDH
SK-N-FI
E
Ad-GFP
Ad-EgIN3 WT Mut
EgIN3: +/+ -/- -/- -/-
BIM-EL
Ad-EgIN3
GAPDH
Primary MEFs
F
siRNA: siSCR siEgIN1 siEgIN2 siEgIN3
BIM-EL
HIF1α
Tubulin
HeLa cells
G
Ad-E3: GFP WT Mut
BIM-EL
cl Casp3
EgIN3
GAPDH
U87
H
Normoxia Anoxia DMSO DMOG DMSO FG0041
EgIN3: +/+ -/- +/+ -/- +/+ -/- +/+ -/- +/+ -/- +/+ -/-
BIM-EL
HIF1α
GAPDH
EgIN3 primary MEF's
I
Adeno: GFP EgIN3
shSCR
shBIM54
shBIM77
U87
shSCR shBIM54 shBIM77
Ad-EgIN3: - + - + - +
Bim-EL
cl-Casp3
EgIN3
GAPDH
U87

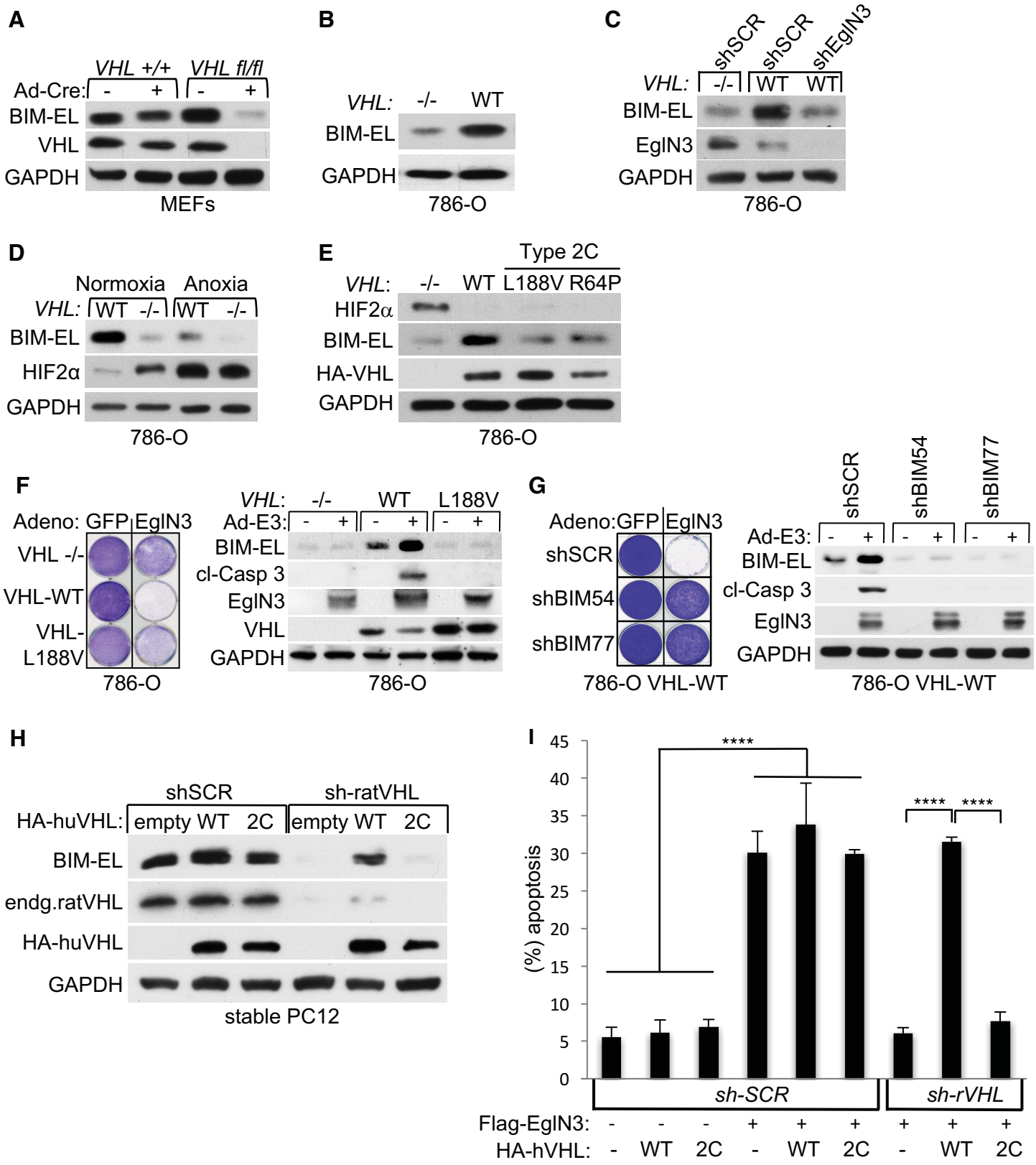
A
VHL +/+
VHL fl/fl
Ad-Cre:
BIM-EL
VHL
GAPDH
MEFs
B
VHL:
BIM-EL
GAPDH
786-O
C
shSCR
shSCR
shEglN3
VHL:
BIM-EL
EglN3
GAPDH
786-O
D
Normoxia
Anoxia
VHL:
BIM-EL
HIF2α
GAPDH
786-O
E
Type 2C
VHL:
HIF2α
BIM-EL
HA-VHL
GAPDH
786-O
F
Adeno:
GFP
EglN3
VHL -/-
VHL-WT
VHL-L188V
786-O
VHL:
Ad-E3:
BIM-EL
cl-Casp 3
EglN3
VHL
GAPDH
786-O
G
Adeno:
shSCR
shBIM54
shBIM77
786-O VHL-WT
Ad-E3:
786-O VHL-WT
H
shSCR
sh-ratVHL
HA-huVHL:
empty
WT
2C
BIM-EL
endg.ratVHL
HA-huVHL
GAPDH
stable PC12
I
(%) apoptosis
sh-SCR
sh-rVHL
Flag-EglN3:
HA-hVHL:
J
Normal adrenal glands
primary human PCC/PGL tumors
VHL mutation
NO 1p36 loss
1p36 loss
21
25
96
108
3
6
16
7
14
36
BIM-EL
GAPDH

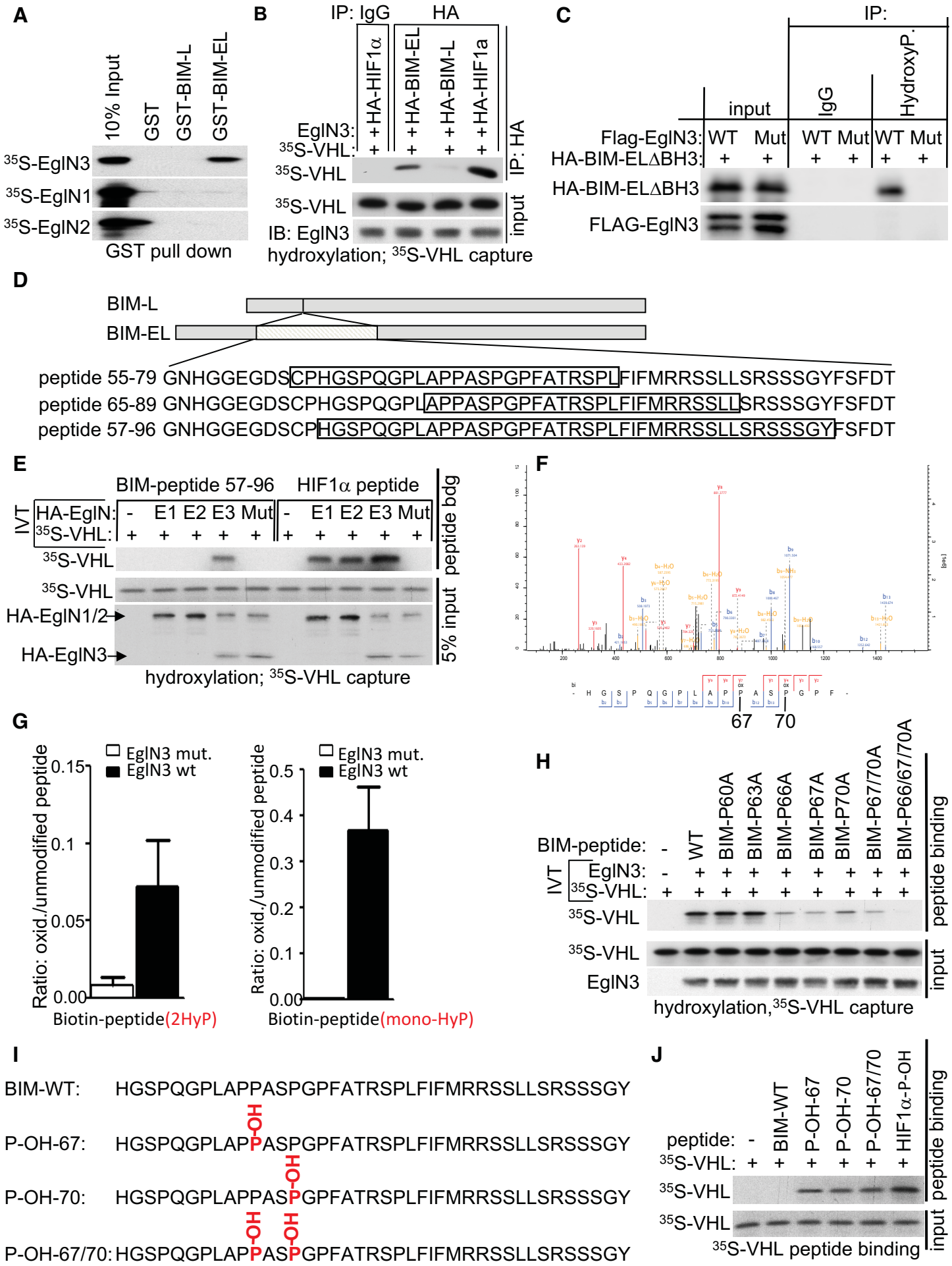
A
10% Input
GST
GST-BIM-L
GST-BIM-EL
35S-EglN3
35S-EglN1
35S-EglN2
GST pull down
B
IP: IgG
HA
EglN3:
35S-VHL:
+HA-HIF1α
+HA-BIM-EL
+HA-BIM-L
+HA-HIF1a
35S-VHL
IB: EglN3
IP: HA
input
hydroxylation; 35S-VHL capture
C
IP:
input
IgG
HydroxyP.
Flag-EglN3: WT Mut WT Mut WT Mut
HA-BIM-ELΔBH3:
HA-BIM-ELΔBH3
FLAG-EglN3
D
BIM-L
BIM-EL
peptide 55-79 GNHGGEGDSCPHGSPQGPLAPPASPGPFATRSPLFIFMRRSSLLSRSSSGYFSFDT
peptide 65-89 GNHGGEGDSCPHGSPQGPLAPPASPGPFATRSPLFIFMRRSSLLSRSSSGYFSFDT
peptide 57-96 GNHGGEGDSCPHGSPQGPLAPPASPGPFATRSPLFIFMRRSSLLSRSSSGYFSFDT
E
BIM-peptide 57-96
HIF1α peptide
IVT
HA-EglN:
35S-VHL:
- E1 E2 E3 Mut - E1 E2 E3 Mut
35S-VHL
peptide bdg
35S-VHL
HA-EglN1/2
HA-EglN3
5% input
hydroxylation; 35S-VHL capture
F
67 70
G
EglN3 mut.
EglN3 wt
Ratio: oxid./unmodified peptide
Biotin-peptide(2HyP)
Biotin-peptide(mono-HyP)
H
BIM-peptide: - WT BIM-P60A BIM-P63A BIM-P66A BIM-P67A BIM-P70A BIM-P67/70A BIM-P66/67/70A
IVT
EglN3:
35S-VHL:
35S-VHL
EglN3
peptide binding
input
hydroxylation,35S-VHL capture
I
BIM-WT: HGSPQGPLAPPASPGPFATRSPLFIFMRRSSLLSRSSSGY
P-OH-67: HGSPQGPLAPPASPGPFATRSPLFIFMRRSSLLSRSSSGY
P-OH-70: HGSPQGPLAPPASPGPFATRSPLFIFMRRSSLLSRSSSGY
P-OH-67/70: HGSPQGPLAPPASPGPFATRSPLFIFMRRSSLLSRSSSGY
J
peptide: - BIM-WT P-OH-67 P-OH-70 P-OH-67/70 HIF1α-P-OH
35S-VHL:
35S-VHL
35S-VHL
peptide binding
input
35S-VHL peptide binding

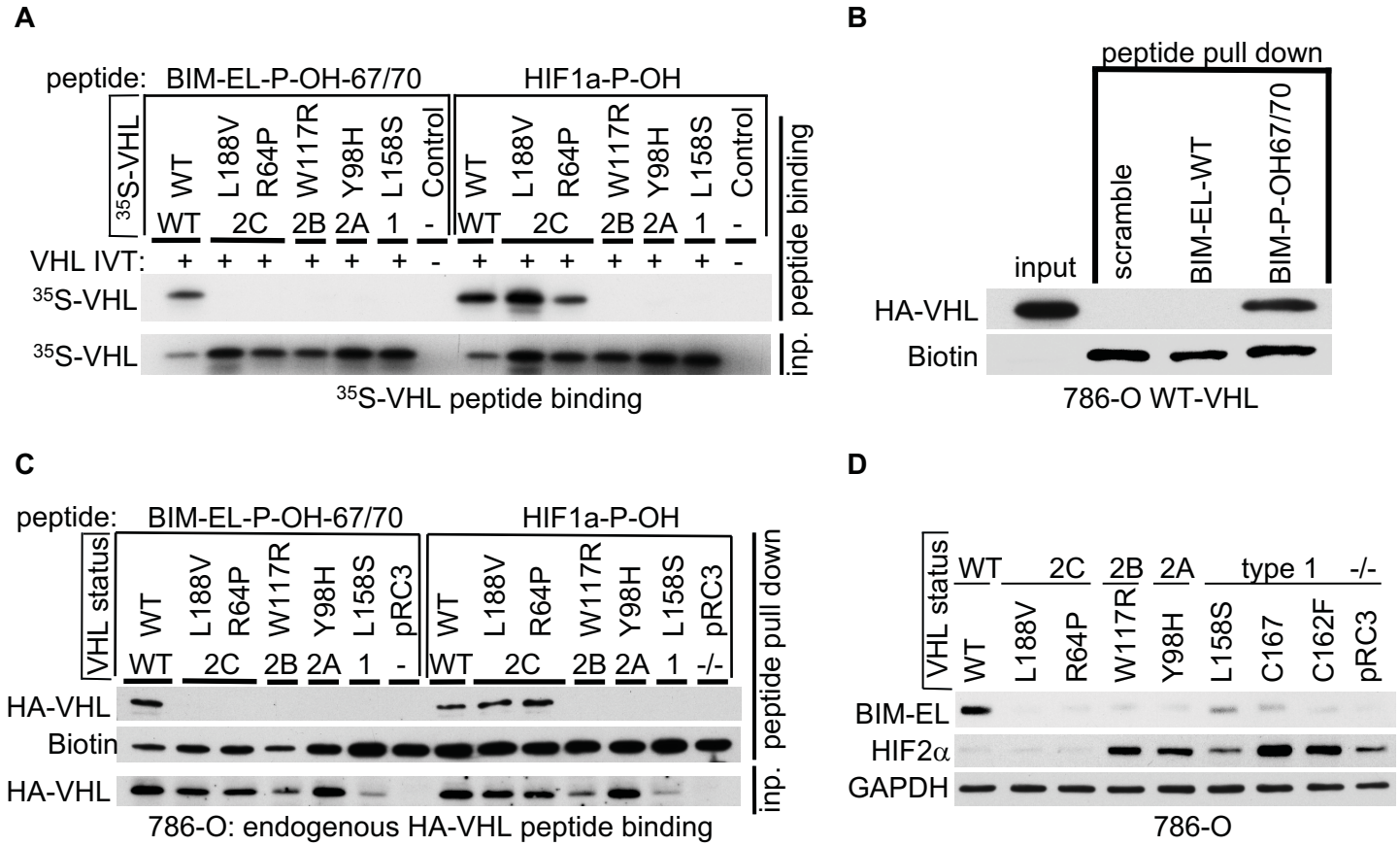
A
peptide: BIM-EL-P-OH-67/70
HIF1a-P-OH
35S-VHL
WT
L188V
R64P
W117R
Y98H
L158S
Control
WT 2C 2B 2A 1 -
VHL IVT:
35S-VHL
peptide binding
inp.
35S-VHL peptide binding
B
peptide pull down
input
scramble
BIM-EL-WT
BIM-P-OH67/70
HA-VHL
Biotin
786-O WT-VHL
C
peptide: BIM-EL-P-OH-67/70
HIF1a-P-OH
VHL status
WT
L188V
R64P
W117R
Y98H
L158S
pRC3
WT 2C 2B 2A 1 -
WT 2C 2B 2A 1 -/-
HA-VHL
Biotin
peptide pull down
inp.
786-O: endogenous HA-VHL peptide binding
D
VHL status
WT 2C 2B 2A type 1 -/-
WT
L188V
R64P
W117R
Y98H
L158S
C167
C162F
pRC3
BIM-EL
HIF2α
GAPDH
786-O

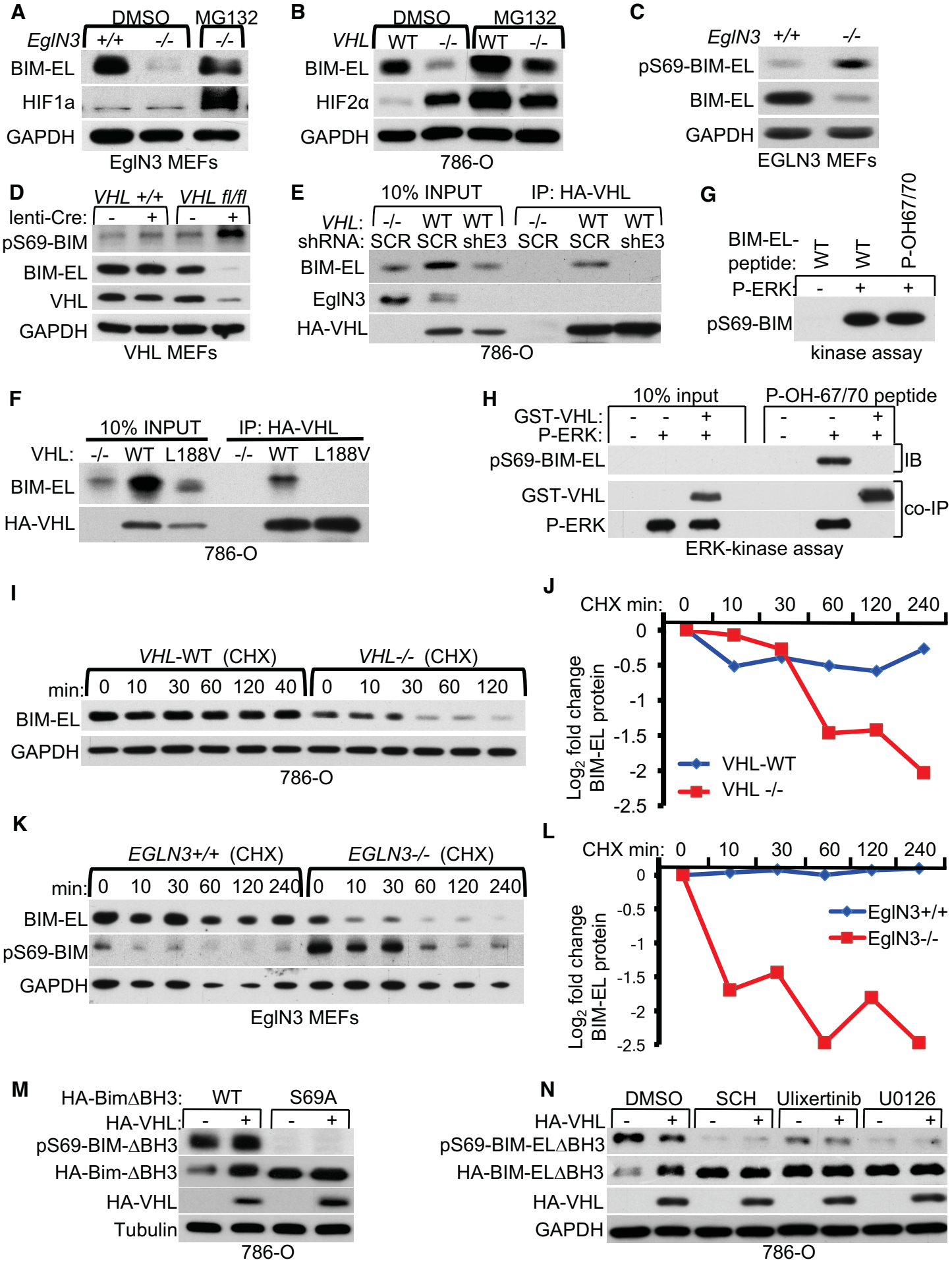
A
DMSO
MG132
EglN3
+/+
-/-
-/-
BIM-EL
HIF1a
GAPDH
EglN3 MEFs
B
DMSO
MG132
VHL
WT
-/-
WT
-/-
BIM-EL
HIF2α
GAPDH
786-O
C
EglN3
+/+
-/-
pS69-BIM-EL
BIM-EL
GAPDH
EGLN3 MEFs
D
VHL +/+
VHL fl/fl
lenti-Cre:
-
+
-
+
pS69-BIM
BIM-EL
VHL
GAPDH
VHL MEFs
E
10% INPUT
IP: HA-VHL
VHL:
-/-
WT
WT
-/-
WT
WT
shRNA:
SCR
SCR
shE3
SCR
SCR
shE3
BIM-EL
EglN3
HA-VHL
786-O
G
BIM-EL-peptide:
WT
WT
P-OH67/70
P-ERK:
-
+
+
pS69-BIM
kinase assay
F
10% INPUT
IP: HA-VHL
VHL:
-/-
WT
L188V
-/-
WT
L188V
BIM-EL
HA-VHL
786-O
H
10% input
P-OH-67/70 peptide
GST-VHL:
P-ERK:
pS69-BIM-EL
IB
GST-VHL
P-ERK
co-IP
ERK-kinase assay
I
VHL-WT (CHX)
VHL-/- (CHX)
min:
0
10
30
60
120
40
0
10
30
60
120
BIM-EL
GAPDH
786-O
J
CHX min:
0
10
30
60
120
240
0
-0.5
-1
-1.5
-2
-2.5
Log2 fold change BIM-EL protein
VHL-WT
VHL -/-
K
EGLN3+/+ (CHX)
EGLN3-/- (CHX)
min:
0
10
30
60
120
240
0
10
30
60
120
240
BIM-EL
pS69-BIM
GAPDH
EglN3 MEFs
L
CHX min:
0
10
30
60
120
240
0
-0.5
-1
-1.5
-2
-2.5
Log2 fold change BIM-EL protein
EglN3+/+
EglN3-/-
M
HA-BimΔBH3:
WT
S69A
HA-VHL:
-
+
-
+
pS69-BIM-ΔBH3
HA-Bim-ΔBH3
HA-VHL
Tubulin
786-O
N
DMSO
SCH
Ulixertinib
U0126
HA-VHL
-
+
-
+
-
+
-
+
pS69-BIM-ELΔBH3
HA-BIM-ELΔBH3
HA-VHL
GAPDH
786-O

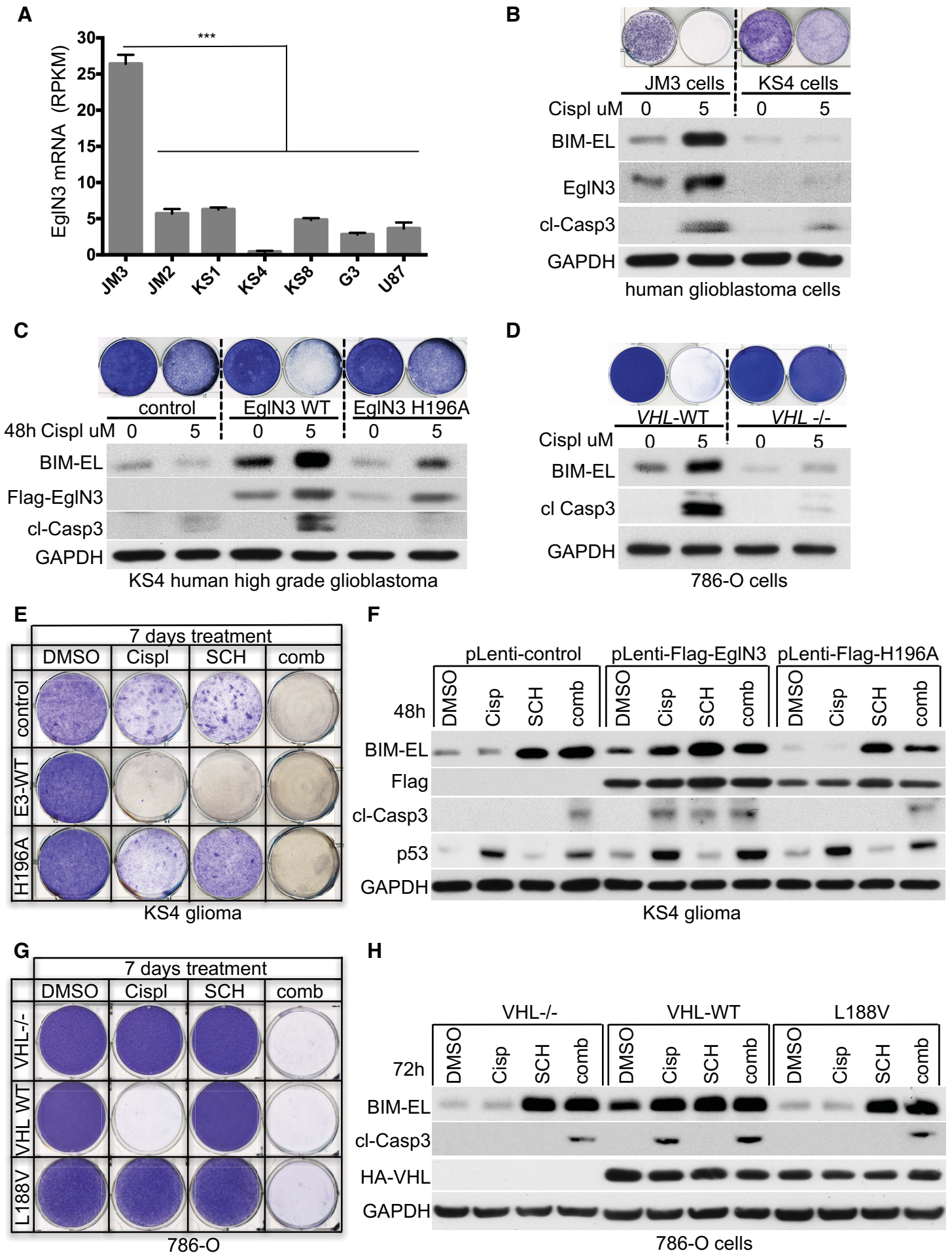
A
EglN3 mRNA (RPKM)
***
JM3
JM2
KS1
KS4
KS8
G3
U87
B
JM3 cells
KS4 cells
Cispl uM
BIM-EL
EglN3
cl-Casp3
GAPDH
human glioblastoma cells
C
control
EglN3 WT
EglN3 H196A
48h Cispl uM
Flag-EglN3
KS4 human high grade glioblastoma
D
VHL-WT
VHL -/-
cl Casp3
786-O cells
E
7 days treatment
DMSO
Cispl
SCH
comb
control
E3-WT
H196A
KS4 glioma
F
pLenti-control
pLenti-Flag-EglN3
pLenti-Flag-H196A
48h
Flag
p53
KS4 glioma
G
VHL-/-
VHL WT
L188V
786-O
H
VHL-/-
VHL-WT
L188V
72h
HA-VHL
786-O cells